

# Dark Matter in Astrophysical Bodies

Joseph Bramante<sup>1</sup>

<sup>1</sup>The Arthur B. McDonald Canadian Astroparticle Physics Research Institute,  
Department of Physics, Engineering Physics, and Astronomy,  
Queen's University, Kingston, Ontario, K7L 2S8, Canada

June 6, 2025

## Abstract

These notes for the IHP summer school introduce dark matter in astrophysical bodies. The flux of dark matter through astrophysical objects is examined from different angles. Dark matter accumulation in these objects is captured in a few derivations. The effects of dark matter on astrophysical objects are briefly illuminated with emphasis on heating signatures and in-situ dark matter core collapse in compact stars.

# Contents

<b>1</b>	<b>Introduction</b>	<b>2</b>
1.1	Examples of Astrophysical Bodies . . . . .	2
<b>2</b>	<b>Flux through Astrophysical Bodies</b>	<b>5</b>
2.1	Tabletop Dark Matter Detection . . . . .	5
2.2	Flux through a sphere . . . . .	7
2.3	Flux through a gravitating sphere . . . . .	8
2.3.1	General Relativistic capture . . . . .	10
2.3.2	Bondi (aka fluid) accretion . . . . .	10
<b>3</b>	<b>Capture by Astrophysical Bodies</b>	<b>11</b>
3.1	Dark matter scatter sensitivity region . . . . .	11
3.2	Single scatter capture in objects . . . . .	13
3.3	Multiscatter capture in objects . . . . .	16
3.4	Redshifted kinetic energy . . . . .	18
<b>4</b>	<b>Thermalization, Heating, and Other Effects in Astrophysical Bodies</b>	<b>18</b>
4.1	First thermalization . . . . .	19
4.2	Second thermalization . . . . .	20
4.3	Heating and other Effects . . . . .	20
<b>A</b>	<b>Kinematics</b>	<b>23</b>
A.1	Elastic scattering review . . . . .	23
A.2	Distribution of recoil energy . . . . .	23

## 1 Introduction

We would like to know about dark matter in astrophysical bodies. Let us begin by reflecting on what is meant by “dark matter in astrophysical bodies.” This is a funny name for a scientific field, since our modern cosmological understanding indicates that pretty much any dark matter can be described as residing “in an astrophysical body,” whether that is the intergalactic medium, a galaxy cluster, a dwarf galaxy (perchance harboring a WIMP-like dark matter halo that sends gamma rays towards a terrestrially orbiting satellite), a main sequence star, a planet, a liquid xenon detector buried kilometers underground, or a crust of bread we left out on the table.

Let’s start by looking at some examples.

### 1.1 Examples of Astrophysical Bodies

- **Liquid Xenon Detectors:** Liquid xenon detectors have been designed to measure the energies of recoiling nuclei for  $E_r \sim \text{keV} - 100 \text{ keV}$ , and particularly to distinguish nuclear and electronic recoils. The typical design includes cryogenic liquid xenon with an applied electric field of  $\sim 25 - 200 \text{ V/cm}$  to drift electrons. Photomultiplier tubes at the top and bottom of the detector readout prompt scintillation photons produced in nuclear recoils and photons produced near the top of the detector, where the ionized and drifted electrons excite gas-phase xenon.

Figure 1 shows recent calibration results from a liquid xenon experiment. Note that the calibration of light and charge yield from nuclear recoils appears to be well-understood for recoils as low as  $E_r \sim 500$  eV.

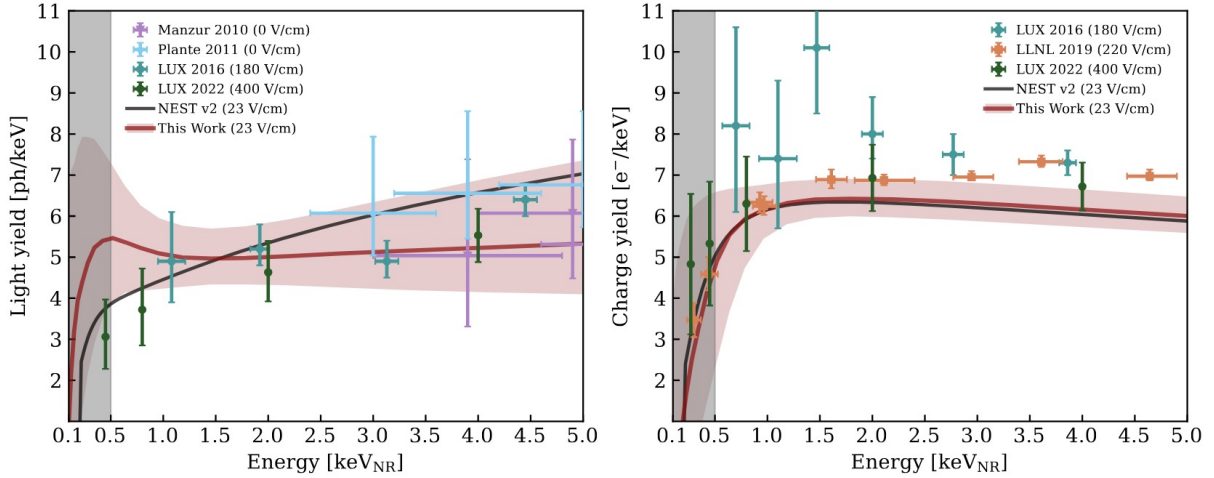


Figure 1: Scintillation and ionization (charge) yields in liquid xenon from [1], calibrated using 154 keV neutrons from a  $^{88}\text{Y}/\text{Be}$  source [2].

- **The Earth:**

A number of dark matter studies have used heat flow through the Earth to constrain dark matter's properties [3–5]. In fact, if all dark matter flowing through the Earth is captured and annihilates in its interior, this would imply  $\sim 3300$  TW of heat emanating from the Earth. This can be compared to an oft-quoted estimate of the Earth's heat flow at around  $44 \pm 1$  TW [6], while a recent analysis by Davies and Davies has suggested a slightly higher heat flux with larger uncertainty,  $47 \pm 2$  TW [7].

Figure 2 shows an Earth heat flow uncertainty map compiled in [7], using thousands of geothermal measurements, and extrapolating these to similar regions under the assumption that regions with similar geology will have similar heat flow.

- **White Dwarfs and Type Ia Explosions:**

White dwarf explosions have been proposed as a means to detect dark matter that would heat their interiors above the temperature required to ignite a thermonuclear explosion [8–11]. This effect must be sought within the context of Type Ia supernovae, which are the explosions of white dwarfs, whose explosion light curves have been instrumental in measurements of cosmic expansion. However, the exact mechanism behind white dwarf explosions is unknown - this is the "Type Ia progenitor problem" [12, 13].

Figure 3 shows the progenitor masses of 337 type Ia supernovae, using the ratio of ejected mass /  $^{56}\text{Ni}$  mass inferred from calibrations using nearby type Ia supernovae. There are also persistent observations of correlations between host galaxy properties and type Ia supernova luminosity [15] (it has been observed that younger galaxies tend to host brighter type Ia supernovae).

In the above examples, we have ordered the astrophysical bodies from most-calibrated to least-calibrated. It is often in these less-calibrated astrophysical bodies that interesting new dark

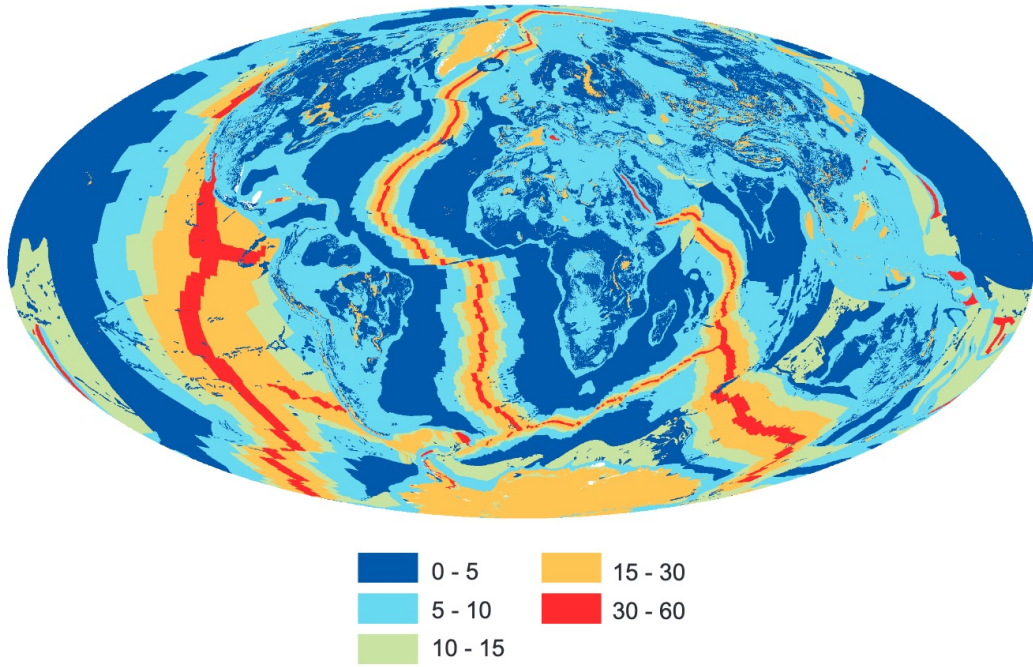


Figure 2: Earth heat flow map uncertainty estimates, in units of  $\text{mW}/\text{m}^2$  [7]. This study found the total heat flow through Earth to be  $47 \pm 2$  TW.

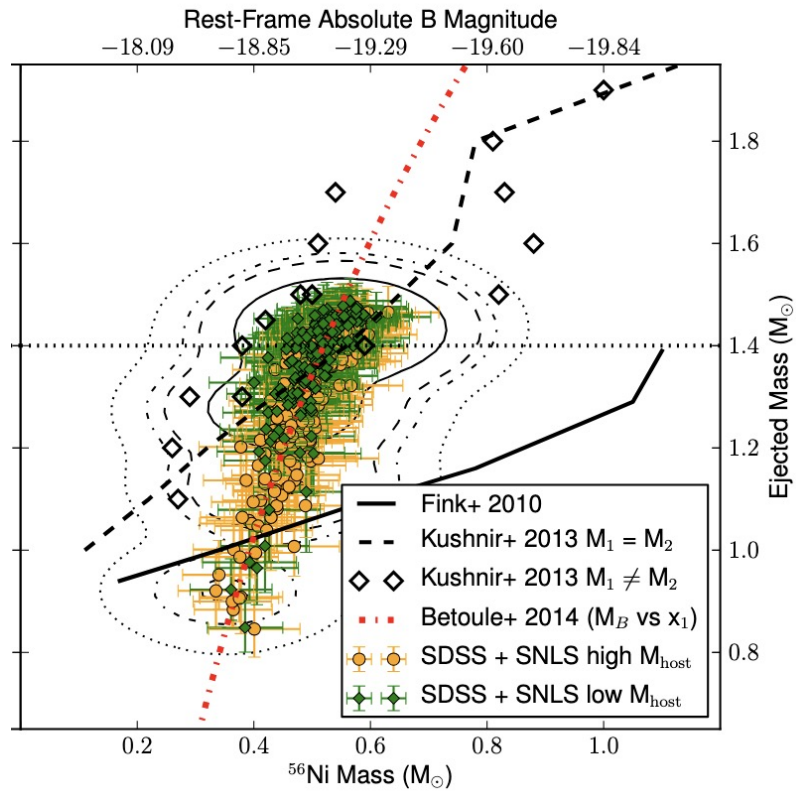


Figure 3: Type Ia supernova progenitor masses inferred from light curve models for the  $^{56}\text{Ni}$  mass as presented in [14].

matter searches are undertaken. To some extent, we might say that every dark matter search method begins as a search for “dark matter in astrophysical bodies,” and then, if there is enough development, becomes refined into a subfield with a distinct name like “direct detection” or “indirect detection with gamma rays.”

## 2 Flux through Astrophysical Bodies

The first research on dark matter’s effect on stars [16–19] began as a means to explain the solar neutrino problem: about two thirds as many electron neutrinos as predicted were observed at the Homestake experiment [20]. For large dark matter-nucleon cross-sections not ruled out by direct detection experiments at the time, it was possible for dark matter captured in the sun to scatter efficiently enough with protons that it would provide an extra conduit for heat flow that reduced nuclear processes like  ${}^8\text{B}$  formation in the center of the sun (and the resulting  ${}^8\text{B}$  neutrino flux).

It is funny that, since the solar neutrino problem was resolved with the discovery that neutrinos have mass, and since massive relic neutrinos contribute a small part of the “dark matter” mass responsible for galactic halos (*e.g.* [21]), then from a certain perspective *we have already discovered the existence of one kind of dark matter, using an anomaly observed in an astrophysical body - the sun.*

Perhaps we will so fortunate again. To begin, we will want to know how much dark matter flows through astrophysical bodies. We will start with astrophysical bodies whose gravitational potentials shouldn’t much alter dark matter’s trajectory.

### 2.1 Tabletop Dark Matter Detection

How much dark matter flows through a table? Since we reside in a (mostly [22, 23]) spherically symmetric dark matter distribution, let us for the moment assume the speed distribution of dark matter is isotropic. The standard Maxwellian halo distribution is given by

$$f(v) \propto v^2 e^{-(v/v_0)^2}, \quad (2.1)$$

which is normalized according to  $\int dv f(v) = 1$ , with a relationship to the halo velocity distribution  $\tilde{f}(\mathbf{v})$ ,

$$f(v) = v^2 \int d\Omega \tilde{f}(\mathbf{v}). \quad (2.2)$$

In practice we will be most interested in the halo flux  $v f(v)$ , which is shown in Figure 4.

To estimate the tabletop flux of dark matter, let us simplify this further and consider an isotropic velocity distribution with single-speed  $v_s = 250$  km/s, which is close to the average speed predicted by current halo models, which find using simulations matching Milky Way parameters that  $v_0 \approx 225$  km/s [22].

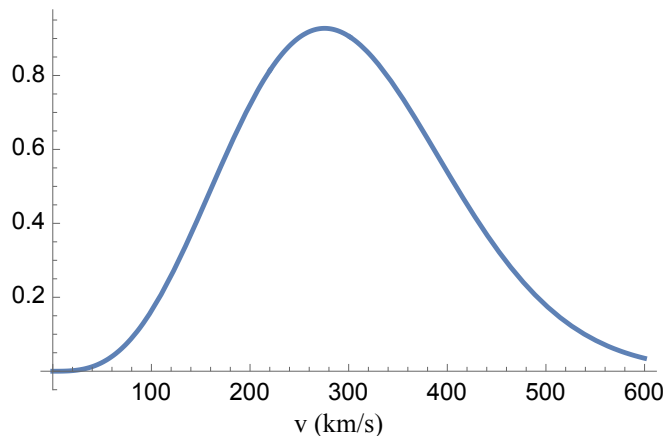


Figure 4: The Standard Maxwellian halo flux distribution  $v f(v)$ . Here the distribution has been normalized according to  $\int dv f(v) = 1$  over the interval  $v \in [0, 600]$  km/s.

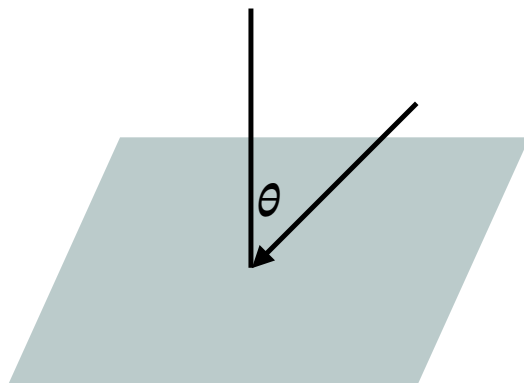


Figure 5: A spherical, isotropic, single-speed dark matter distribution moves through the table. We compute the flux through the top of the table.

In Figure 5 we show a diagram for the flux of isotropic, single-speed dark matter flowing through the top of a table. The flux  $\mathbf{F}$  (units per area per time) of dark matter with density  $n_\chi$  through the top of the table for a spherical, isotropic, single-speed  $v_s$  distribution is

$$|d\mathbf{F}| = \frac{1}{2} n_\chi dv_z = \frac{1}{2} n_\chi v_s \cos \theta \sin \theta d\theta \quad (2.3)$$

where we have used that the fraction of spherically distributed dark matter flowing through the flat tabletop surface is proportional to  $v_s \cos \theta$ , and we integrate over  $\theta$  (note that the factor of  $\frac{1}{2}$  actually comes from integrating the azimuthal angle and dividing by  $4\pi$  steradians,  $\int d\phi/4\pi = \frac{1}{2}$ , see below). Integrating over the tabletop and spherical distribution we obtain the integrated mass flux  $d\mathcal{F} = d\mathbf{F} \cdot d\mathbf{A}$  through the table with area  $A$ ,

$$\mathcal{F} = \frac{A n_\chi v_s}{2} \int_0^{\pi/2} \cos \theta \sin \theta d\theta = \frac{A n_\chi v_s}{4} . \quad (2.4)$$

Let us now find the same result with more formality. If the velocity distribution  $\tilde{f}(\mathbf{v})$  of dark matter is isotropic then this implies using Eq. (2.2),

$$\begin{aligned} f(v) &= v^2 \int d\Omega \tilde{f}(\mathbf{v})^{(iso)} = 4\pi v^2 \tilde{f}(\mathbf{v})^{(iso)} \\ &\rightarrow \tilde{f}(\mathbf{v})^{(iso)} = \frac{f(v)}{4\pi v^2}, \end{aligned} \quad (2.5)$$

We define the vector flux

$$d\mathbf{F}(\mathbf{v}) = n_\chi f(\mathbf{v}) \mathbf{v} d^3v,$$

and the differential area element with normal vector  $\hat{n}$

$$d\mathbf{A} = \hat{n} dA.$$

Then the integrated flux  $\mathcal{F}$  through a flat surface oriented in the  $x - y$  plane, with area  $A$  is

$$\mathcal{F} = \int d^3v \int_A d\mathbf{A} \cdot d\mathbf{F}(\mathbf{v}) = A n_\chi \int_{v_z < 0} d^3v \tilde{f}(\mathbf{v}) v \cos \theta.$$

Switching to spherical velocity coords  $(v, \theta, \phi)$ , with  $v_z \equiv v \cos \theta$ ,

$$d^3v = v^2 dv \sin \theta d\theta d\phi,$$

using the expression (2.5) for an isotropic velocity distribution and integrating over the bottom hemisphere of flux oriented towards our tabletop  $\theta \in [0, \frac{\pi}{2}]$ ,  $\phi \in [0, 2\pi]$  gives

$$\begin{aligned} \mathcal{F} &= A n_\chi \int_0^\infty dv v^3 \frac{f(v)}{4\pi v^2} (2\pi) \int_0^{\pi/2} \cos \theta \sin \theta d\theta \\ &= \frac{1}{4} A n_\chi \int_0^\infty dv f(v) v = \frac{1}{4} n_\chi \langle v \rangle A, \end{aligned}$$

where we note that the expectation value of  $v$  for speed distribution  $f(v)$  is defined by  $\langle v \rangle = \int_0^\infty dv f(v) v$ . Hence,

$$\boxed{\mathcal{F} = \frac{1}{4} n_\chi \langle v \rangle A.} \quad (2.6)$$

Note that this is valid for any isotropic flux, and we see that the simple estimate above which used a single-speed velocity  $v_s$ , is actually valid for a generalized isotropic halo model with the replacement  $v_s \rightarrow \langle v \rangle$ . In terms of mass density  $\rho_\chi = m_\chi n_\chi$ , the tabletop mass flux is also just

$$\boxed{\dot{M} = \frac{1}{4} \rho_\chi \langle v \rangle A.}$$

## 2.2 Flux through a sphere

We now compute the inward flux through a spherical surface of radius  $R$ . As before, we define the vector differential flux

$$d\mathbf{F}(\mathbf{v}) = n_\chi f(\mathbf{v}) \mathbf{v} d^3v,$$

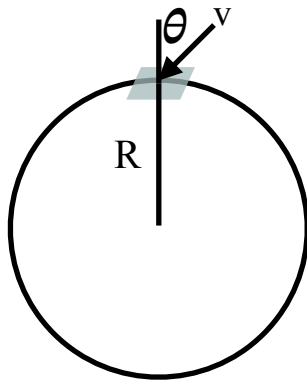


Figure 6: A dark matter flux moving through the sphere.

and have an area element

$$d\mathbf{A} = \hat{n} dA, \quad dA = R^2 \sin \theta_s d\theta_s d\phi_s,$$

with  $\hat{n}$  the normal vector.

Figure 6 shows the flux of dark matter through the sphere.

We see from the definitions above that the dot product of the differential flux  $d\mathbf{F}$  with the sphere's surface element  $d\mathbf{A}$  will have the same form and dependence on the angle  $\theta$  as for the tabletop flux calculation. Hence to compute the integrated flux through the sphere we may simply replace the area of the tabletop in (2.6) with the area of the sphere.

$$\mathcal{F} = \pi R^2 n_x \langle v \rangle. \quad (2.7)$$

### 2.3 Flux through a gravitating sphere

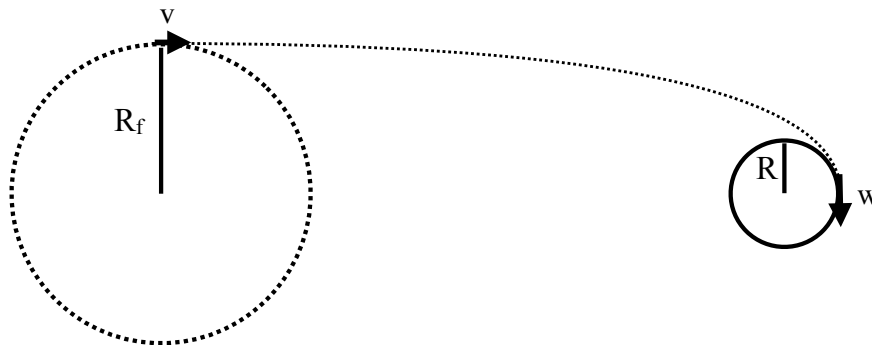


Figure 7: Dark matter deflected towards a star, with an effective “flux sphere” of radius  $R_f$ . The trajectory shown is the limiting case that the particle has an angular momentum which results in it just grazing the surface of the star.

In the case of a gravitating sphere (let's call it a star), the incoming dark matter will be deflected towards the star. Assuming the incoming flux of dark matter is spherically distributed, it follows from spherical symmetry that there is an effective ‘‘capture sphere’’ surrounding the star.

Figure 7 shows the effective flux sphere and the limiting case that a dark matter particle is deflected just enough to graze the surface of the star.

To estimate the flux sphere radius  $R_f$ , let us analyze the limiting case of a dark matter particle with halo speed  $v$ , on a trajectory that will cause it to barely graze the surface of the star. Conservation of energy implies the velocity of such a trajectory grazing the surface of the star is

$$w^2 = v^2 + v_{esc}^2,$$

while conservation of angular momentum implies

$$wR = vR_f$$

where  $v_{esc}^2 = 2GM/R$ . Altogether this implies a flux radius for the star of  $R_f = R \frac{w}{v}$ , implying a flux through the star

$$\mathcal{F} = \pi R_f^2 n_\chi v, = \pi R^2 n_\chi \frac{w^2}{v}. \quad (2.8)$$

In more detail, we assume a homogeneous dark-matter density  $n_\chi$  far from the star, with speed  $v$ . Particles with impact parameter  $b$  will have specific angular momentum  $J = jm$  relative to the star

$$j = bv.$$

By energy conservation, at a far distance from the star  $E = \frac{1}{2}mv^2$ , while at radial distance  $r$  from the star,

$$\frac{E}{m} = \frac{1}{2}\dot{r}^2 + \frac{j^2}{2r^2} - \frac{GM}{r},$$

where the second term is the initial kinetic energy re-expressed as angular momentum.

At the point of closest approach on its hyperbolic trajectory the particle will have vanishing radial velocity so

$$\frac{1}{2}v^2 = \frac{j^2}{2r_{\min}^2} - \frac{GM}{r_{\min}},$$

where we substituted in its initial halo energy  $E$ . Requiring that the particle grazes the star's surface fixes  $r_{\min} = R$ , which in turn fixes the maximum angular momentum

$$j_{\max}^2 = 2R^2 \left( \frac{1}{2}v^2 + \frac{GM}{R} \right) = R^2 \left( v^2 + v_{esc}^2 \right),$$

which gives the maximum impact parameter in terms of  $j_{\max} = b_{\max}v$  as

$$b_{\max} \equiv R_f = R \sqrt{\frac{v^2 + v_{esc}^2}{v^2}}.$$

### 2.3.1 General Relativistic capture

If the star is sufficiently compact so that  $v_{esc}$  is close to relativistic, General Relativistic corrections to the effective flux radius will apply.

The effective flux radius corrections from General Relativity can be arrived at as follows. The arguments leading to Eq. (2.9) are the same, but the angular momentum of the particle grazing the star picks up a factor of  $\gamma_{v_{esc}} = \frac{1}{\sqrt{1-v_{esc}^2}}$  (in the limit  $v_{esc} \gg v$ ). (One way to understand this shift in the angular momentum is to note that in the rest frame of a distant observer, the radius of the neutron star will appear a factor of  $\gamma_{v_{esc}}$  larger due to the bending of light.) This implies the effective flux through a compact star is

$$\mathcal{F} = \pi R^2 \gamma_{v_{esc}}^2 n_X \frac{v_{esc}^2}{v}. \quad (2.9)$$

### 2.3.2 Bondi (aka fluid) accretion

A way to understand fluid accretion relative to particle accretion is to realize that at a certain radius from a star, any accreting fluid element will meet an equal and opposite momentum fluid element, assuming the fluid is isotropic and homogeneous around the star. At this radius the angular momentum of the fluid relative to the star cancels against its matching fluid element, and the fluid becomes bound to the star.

This radius is known as the Bondi radius, and is illustrated in Figure 8.

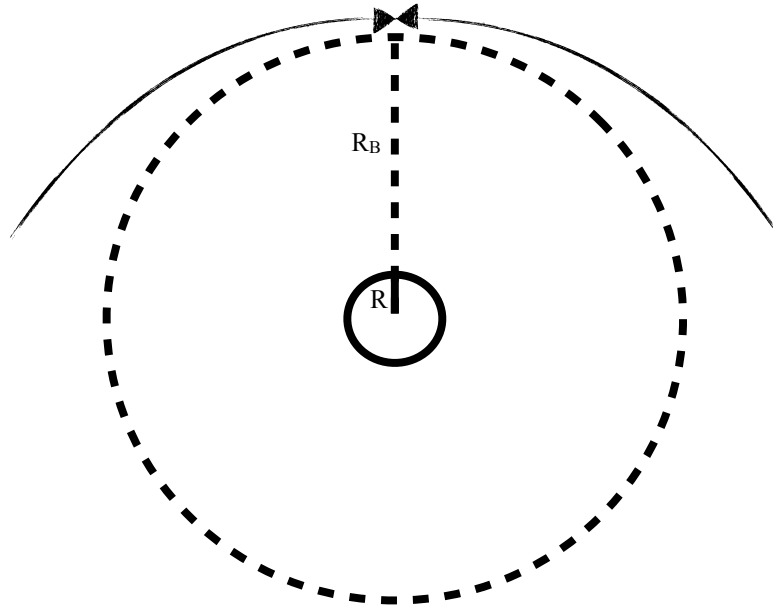


Figure 8: At a certain radius from the star, gravitational deflection implies each fluid element of a homogeneous and isotropically distributed fluid will collide with a fluid element with opposite momentum.

The radius at which we can expect an  $\mathcal{O}(1)$  gravitational deflection of a fluid element is where the fluid's halo kinetic energy is equal to the energy it has gained falling into the star,

$$\frac{1}{2}mv^2 \approx \frac{GMm}{R_B}, \quad (2.10)$$

from which we can immediately obtain the Bondi radius  $R_B = R \frac{v_{esc}^2}{v^2}$ . This implies the effective Bondi flux is

$$\mathcal{F} = \pi R^2 n_\chi \frac{v_{esc}^4}{(v^2 + c_s^2)^{3/2}}, \quad (2.11)$$

where here we have accounted for the fact that the fluid flow may be supersonic or subsonic at the Bondi radius by making the replacement  $v \rightarrow \sqrt{v^2 + c_s^2}$ , where  $c_s$  is the fluid sound speed [24].

In a more detailed derivation of Bondi accretion, the above argument is formalised using Euler's equation for an inviscid fluid (aka momentum conservation for a fluid), along with the mass continuity equation. When combined, the resulting expression has a number of solutions, some of which imply the fluid's radial velocity vanishes at the Bondi radius. Both supersonic and subsonic fluid flow solutions are represented in Eq. (2.11). However, some caution is advisable when using the Bondi accretion estimate - the Bondi formalism does not account for detailed fluid dynamics, *e.g.* turbulence.

### 3 Capture by Astrophysical Bodies

Let us turn to capture of dark matter in astrophysical bodies. So far we have obtained expressions for the flux of dark matter through stars (/planets/tables/etc), but now we want to know what amount of the dark matter flux through the star becomes gravitationally bound to the star.

#### 3.1 Dark matter scatter sensitivity region

We'll begin by reviewing the dark matter scatter parallelogram (or triangle in the case of multi-scatter), shown in Figure 9. This sketches out the region of sensitivity objects have for dark matter that scatters with their interiors.

- **Left, single scatter:** There will be some threshold energy  $E_{th}$  the object is sensitive to. In the case that the object is sensitive to single scatter recoil interactions with dark matter, this will define the left edge of the parallelogram and is parametrically determined by the energy transferred in a single scattering event

$$E_{th} \sim \mu_{a\chi} v^2, \quad (3.1)$$

where the particle (nucleus, electron) dark matter scatters with has a mass  $m_a$  and  $\mu_{a\chi}$  is the reduced mass.

- **Bottom, single scatter:** If the object is sensitive to single-scatter interactions from dark matter, the bottom edge will scale with dark matter particle flux  $n_\chi \propto \frac{\rho_\chi}{m_\chi}$ .

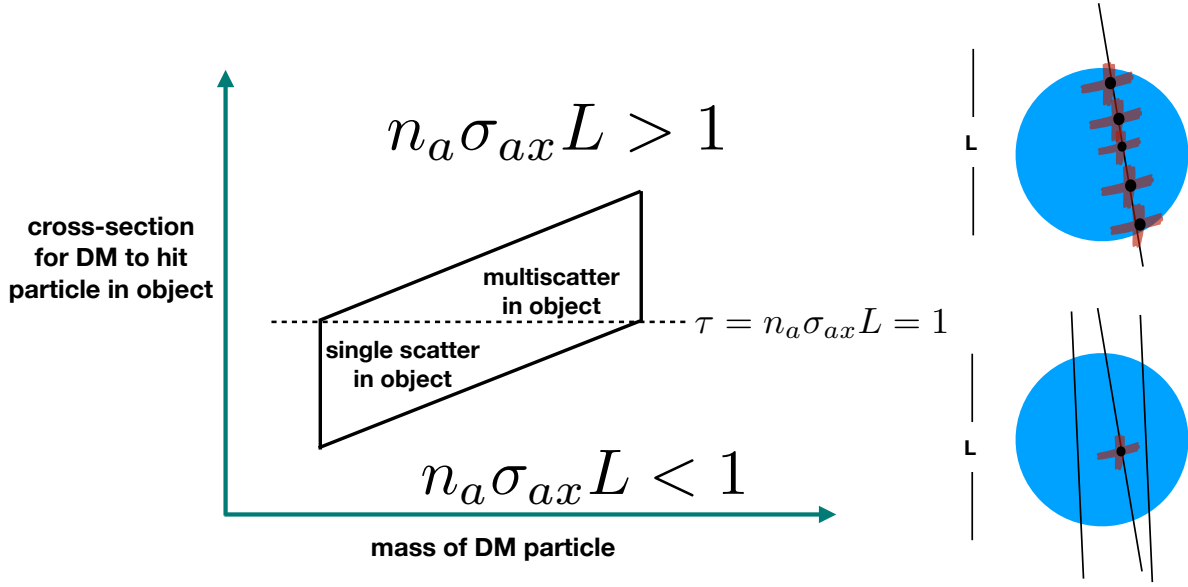


Figure 9: The dark matter detection scattering sensitivity region is shown. The left/bottom edges are defined by the energy threshold of the detector. The right edge is determined by the total dark matter flux through the detector. The top edge is defined by overburden attenuation.

- **Bottom, multiscatter:** If the object is only sensitive to multiple-scatter interactions from dark matter, the bottom edge will be determined by the threshold energy of dark matter, which will depend on the energy transferred per scatter and the optical depth (aka number of scatters)  $\tau \sim n_a \sigma_{a\chi} L$ .

$$E_{th} \sim \mu_{a\chi} v^2. \quad (3.2)$$

- **Right:** The minimum flux of dark matter required for the objects sensitivity defines the right edge of the parallelogram. In the case that the object is sensitive to a  $F_{min}$  dark matter particles transiting through the detector, this will be

$$F_{min} \sim A_{obj} n_{\chi} \langle v \rangle \quad (3.3)$$

$$\rightarrow m_{\chi} \sim A_{obj} n_{\chi} \langle v \rangle / F_{min}. \quad (3.4)$$

In the case of a mostly background-free dark matter detector, 90% confidence bounds usually set  $F_{min} = 2.4$

- **Top:** The top edge of the sensitivity zone is often called the overburden or “overburden attenuation” boundary. This is where dark matter interactions with material around the object deplete dark matter particle energy so that it can no longer impart the threshold energy  $E_{th}$ . Parametrically this is determined by (assuming  $m_{\chi} \gg m_a$ )

$$E_{th} \sim m_{\chi} v^2 \left( 1 - \frac{m_a}{m_{\chi}} \right)^{\tau_o}, \quad (3.5)$$

where the number of scatters in overburden of length  $L_o$  is  $\tau_o \sim n_{a,o} \sigma_{a\chi} L_o$ . For many objects this will scale with  $1/m_{\chi}$ , because the binomial expansion of the RHS of Eq. (3.5) will be  $m_{\chi} v^2 [1 - \tau_o m_a / m_{\chi} + \mathcal{O}(\tau_o^2 m_a^2 / m_{\chi}^2) \dots]$ .

### 3.2 Single scatter capture in objects

Now that we've catalogued some ways dark matter interacts with astrophysical objects, let's compute how much dark matter passing through a star becomes gravitationally bound to the star through scattering.

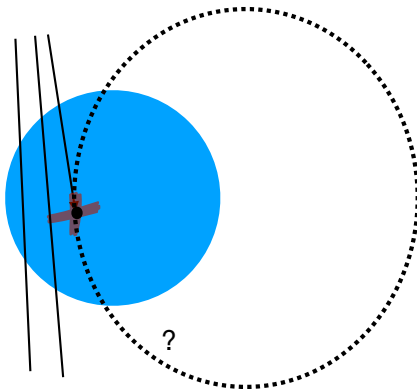


Figure 10: Single scatter capture.

To estimate the rate at which dark matter will become gravitationally bound to an astrophysical object, in the “single scatter” (*i.e.*  $\tau \ll 1$ ) regime, we combine the flux for dark matter through the object  $\mathcal{F}$  with the probability for a single scatter during the dark matter trajectory through the star  $p_1 \sim \tau_R \sim n_a \sigma_{a\chi} R$ , with the probability for a single scatter to slow the dark matter below escape velocity  $g_1$ :

$$\frac{dN_\chi}{dt} \equiv C_\chi \sim \pi R^2 \frac{v_{esc}^2}{v_s} p_1 g_1. \quad (3.6)$$

It remains to estimate  $g_1$ . Assuming for the moment that the speed through the star is much larger than the DM halo velocity,  $v_{esc} \gg v$ , the requirement for DM to be captured is that its energy loss in the scatter  $\Delta E$  is greater than its halo kinetic energy  $E = \frac{1}{2} m_\chi v^2$ , where its energy crossing the star is here approximated as  $E_0 \sim \frac{1}{2} m_\chi v_{esc}^2$ .

A kinematic analysis (see later text) shows that for elastic scattering the energy loss in the star's rest frame is evenly distributed over the interval

$$0 < \Delta E < E^{max} = E\beta_+, \quad (3.7)$$

where  $\beta_+ \equiv 4m_a m_\chi / (m_a + m_\chi)^2$ . It follows from this that the probability for the dark matter to lose  $E = \frac{1}{2} m_\chi v^2$  in one scatter is

$$g_1 \sim \frac{1}{\beta_+} \left( \beta_+ - \frac{v^2}{v_{esc}^2} \right), \quad (3.8)$$

where the factor of  $\frac{1}{\beta_+}$  normalizes the range of energy losses equally over  $0 < \Delta E < E^{max}$ .

Let us now proceed with a full single scatter derivation for the capture of dark matter on stars. What follows is an abridged version of a derivation given Appendix A of [25], where this procedure was first detailed in [17, 19]. Let us lay out the steps we will follow in this derivation:

- A. At a distance from the star where the dark matter particles are all Boltzmann distributed according (2.2), we can expect that half the dark matter particles will have a trajectory that crosses the “effective flux sphere” of the star. These will be particles with headings over angular range  $-\pi/2 < \theta < \pi/2$ , with  $\theta$  defined from a normal vector or radius pointing away from the star’s center. As before we will take the integrated flux of dark matter to be defined by  $\mathcal{F}$ .
- B. To determine the trajectories of the particles through the star, we will be using the same principle as in Section 2.3, that conservation of angular momentum will dictate how close the dark matter passes to the star’s center. In this derivation we will explicitly integrate over incoming angular momenta of the dark matter particles to obtain the precise velocity-weighted flux of dark matter in the star’s interior.
- C. To further specify our procedure, we will be integrating over spherical shells of our star with thickness  $dr$ . Within each of these shells, we can determine the precise velocity-weighted flux of dark matter using angular momentum conservation. In addition, in each of these star shells we can use the number density of particles  $n(r)$  that the dark matter can scatter with, to determine a probability for capture as the dark matter crosses the shell.

As we have seen in prior sections, sufficiently far away from the star the dark matter particles will follow a Maxwell Boltzmann halo distribution, which here we will label with velocity  $u$ , where we define this formally over interval  $u$  to  $u + du$  as

$$f(u)du = \frac{6\sqrt{3}}{\sqrt{\pi}} \frac{n_\chi u^2}{\bar{v}^3} \text{Exp} \left[ -\frac{3u^2}{2\bar{v}^2} \right] du, \quad (3.9)$$

where the numerical prefactors enforce the normalization indicated for the halo distribution (2.2) in prior sections, and we retain the rescaled velocity dispersion  $v_0^2 = \frac{2}{3}\bar{v}^2$  as a historic convention.

At a radius  $r$  from the star, each particle will have a total velocity given by  $w^2 = u^2 + v_e^2(r)$ , where we define  $v_e(r)$  here as the escape velocity from the star at radius  $r$ . Then following the same logic and procedure as Section 2.1 we know that the (non-integrated) flux of dark matter through the effective capture sphere far from the star is given by

$$|d\mathbf{F}| = \frac{1}{2}u f(u) du \cos \theta d(\cos \theta) = \frac{1}{4} f(u)u du d(\cos^2 \theta). \quad (3.10)$$

As before this is related to the integrated flux for an a distant radius  $R_a$  through,

$$d\mathcal{F} = 4\pi R_a^2 dF = \pi R_a^2 f(u)u du d(\cos^2 \theta). \quad (3.11)$$

We will use each particle’s angular momentum to determine its trajectory across a spherical shell at distance  $r$  from the center of the star. We can temporarily introduce angle  $\alpha$  between the dark matter’s velocity  $\mathbf{w}$  and the normal vector on the surface of the sphere  $\hat{n} = \hat{r}$ . Then matching

the angular momentum of the dark matter at the effective flux radius to the angular momentum at shell radius  $r$ ,

$$J \equiv uR_a \sin \theta = wr \sin \alpha. \quad (3.12)$$

As defined previously,  $w^2 = u^2 + v_e^2(r)$ , where  $v_e(r)$  is the radius  $r$  escape speed. Using  $dJ^2 = u^2 R_a^2 d(\cos^2 \theta)$ , we re-express the flux

$$d\mathcal{F} = \pi f(u) \frac{du}{u} dJ^2. \quad (3.13)$$

We again define the probability of dark matter to become orbitally bound to the star after scattering once as  $g_1(w)$ . The probability for dark matter for dark matter to be captured while traversing a spherical shell of width  $dl = dr/\cos \alpha$ , is then given by

$$n_a(r) \sigma_{a\chi} g_1(w) dl, \quad (3.14)$$

where  $n_a$  is the usual number density of particles the dark matter scatters with.

We can further use the relation in Eq. (3.12) to relate the length differential to the angular momentum,  $dl = dr/\sqrt{1 - (J/rw)^2}$ . With all of this, the differential single scatter capture rate is found by taking the product of Eqs. (3.14) and (3.13), and then accounting for all the incoming angles of the dark matter flux by integrating over  $J$ . Finally, reminiscent of the limiting case for grazing the a spherical shell that we studied in Section 2.3, we must implement a theta function to enforce that the incoming flux has small enough angular momentum that it passes through a shell of size  $r$ ,  $\Theta(rw - J)$ ,

$$\begin{aligned} dC_1 &= 4\pi n_a(r) \sigma_{a\chi} g_1(w) f(u) \frac{du}{u} \int_0^\infty dJ \Theta(rw - J) J dl \\ &= 4\pi n_a(r) \sigma_{a\chi} g_1(w) f(u) \frac{du}{u} w^2 r^2 dr, \end{aligned} \quad (3.15)$$

Note that here we also multiplied by a factor of 2 to account for the particle passing through both sides of the spherical shell.

The probability for capture after a single scatter still needs to be determined, which we have defined as  $g_1(w)$ . In Appendix A we review kinematics relevant for elastic scattering in the star's rest frame. That kinematic analysis demonstrates that per scatter, the fraction of kinetic energy lost will be distributed equally over an interval  $0 < \Delta E/E_i < \beta_+$ , for initial kinetic energy  $E_i = \frac{1}{2}m_\chi w^2$ , with the kinematic factor  $\beta_+$  defined as

$$\beta_\pm \equiv \frac{4m_\chi m}{(m_\chi \pm m)^2}, \quad (3.16)$$

In order for dark matter to be captured after a single scatter, it should lost a fraction  $u^2/w^2$  of its energy  $E_i$ , since this means it will have lost the kinetic energy it had before being deflected towards the star. Hence the probability for capture after a scatter  $g_1(w)$  is given by the probability for the energy loss fraction to be greater than the ratio of the halo kinetic energy to the kinetic energy at radius  $r$ ,  $u^2/w^2$ ,

$$\frac{1}{\beta_+} \left( \beta_+ - \frac{u^2}{w^2} \right), \quad (3.17)$$

and to this we must multiply by a theta function that enforces the capture condition is fulfilled after one scatter,

$$\Theta\left(\beta_+ - \frac{u^2}{w^2}\right). \quad (3.18)$$

So then in total  $g_1(w)$  is Eqs. (3.17) and (3.18) multiplied together. Putting this finally into Eq. (3.15), the single scatter capture as a function of radius (performing the  $u$  integral), is

$$C_1 = \pi \sqrt{\frac{96}{\pi}} \frac{n_X}{\bar{v}} \int_0^R dr r^2 n_a(r) \sigma_{a\chi}(r) v_e^2(r) \left(1 - \frac{1 - e^{-A^2(r)}}{A^2(r)}\right), \quad (3.19)$$

where there is a Boltzmann variable  $A^2 \equiv 3v_e^2(r)/2\bar{v}^2\beta_-$ . If we ignore the radial dependence of the star's density profile, and set  $v_e(r) \simeq v_{esc} \equiv v_e(R)$ , the result is

$$C_1 \simeq \sqrt{6\pi} R^2 \frac{\rho_\chi}{m_\chi} \frac{v_{esc}^2}{\bar{v}} \text{Min} \left[1, \frac{\sigma_{a\chi}}{\sigma_{sat}}\right] \left(1 - \frac{1 - e^{-A^2}}{A^2}\right), \quad (3.20)$$

where  $\sigma_{sat} \equiv \frac{\pi R^2}{N_a}$ , with  $N_a$  the number of particles  $a$  in the star. The Min function is introduced to limit the amount of dark matter captured to not be greater than the flux of dark matter through the star (without this, as  $\sigma_{a\chi}$  increases, eventually the equation would predict more capture than the flux through the star).

### 3.3 Multiscatter capture in objects

When the cross-section for dark matter to scatter is high enough,  $\sigma_{a\chi} \gtrsim \sigma_{sat}$ , dark matter will scatter multiple times as it crosses the star. This requires a somewhat different set of calculations to compute capture. Here we will present a very abridged presentation of results detailed in [25].

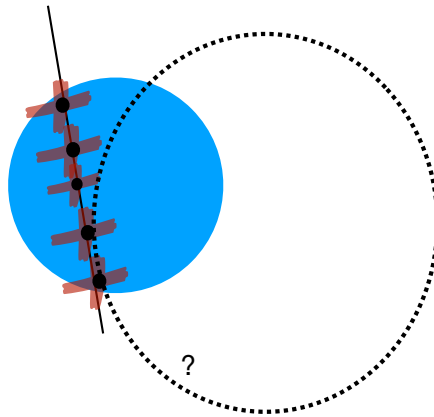


Figure 11: Multiscatter capture.

For the purposes of computing multiscatter capture it will be convenient to specify a generalized optical depth as  $\tau = \frac{3\sigma_{a\chi}}{2\sigma_{\text{sat}}}$ , which is the average number of times dark matter scatters when traversing the star.<sup>1</sup>

For the simplest multiscatter dark matter analysis, we begin by analyzing dark matter's interactions when it enters the star at radius  $R$ . Specifying  $y$  as the cosine angle between the star's radius and dark matter's trajectory as it enters the star, the probability for dark matter to scatter  $N$  times as it passes through the star integrated over all incidence angles ( $y$ ) is

$$p_N(\tau) = 2 \int_0^1 dy \frac{y e^{-y\tau} (y\tau)^N}{N!}, \quad (3.22)$$

which is a Poisson distribution modified to account for the dark matter's trajectory through the star.

Then the multiscatter capture rate, defined as the capture rate for dark matter to become bound after exactly  $N$  scatters is given by

$$C_N = \pi R^2 p_N(\tau) \int_0^\infty f(u) \frac{du}{u} w^2 g_N(w), \quad (3.23)$$

Notice that we have not yet defined the probability that the dark matter loses enough energy to be captured after  $N$  scatters  $g_N(w)$ . In order to accommodate the eventual form of this probability, it is useful for us to shift to an integral over  $w$ , where  $w^2 = u^2 + v_{\text{esc}}^2$ . With this shift the capture rate becomes

$$C_N = \pi R^2 p_N(\tau) \int_{v_e}^\infty dw \frac{f(u)}{u^2} w^3 g_N(w), \quad (3.24)$$

where to obtain the total capture rate we must sum over the possibility that capture occurs for any number of scatters  $C_N$

$$C_{\text{tot}} = \sum_{N=1}^\infty C_N. \quad (3.25)$$

Usually this sum is truncated at an appropriate  $C_N$  value, for which the capture is sufficiently miniscule.

The probability that enough energy will be lost after  $N$  scatters for capture depends on the initial dark matter velocity at the surface of the star  $w$ , since the initial energy is  $E_0 = m_\chi w^2/2$ . Using somewhat different notation, the energy lost per scatter (see Appendix A) is given by  $\Delta E = z\beta_+ E_0$ , where  $z$  stands in for the CM scattering angle and ranges over  $z \in [0, 1]$ . After  $N$  scatters, the energy and velocity will become

$$E_N = \prod_{i=1}^N (1 - z_i \beta_+) E_0, \quad v_N = \prod_{i=1}^N (1 - z_i \beta_+)^{1/2} w. \quad (3.26)$$

---

<sup>1</sup>The  $\frac{3}{2}$  factor in the optical depth comes from setting the optical depth to one for dark matter traversing a path  $2R$ ,

$$1 = n \sigma_{a\chi} (2R) = \frac{N_a}{(4/3)\pi R^3} \sigma_{a\chi} (2R) = \frac{3 N_a}{2\pi R^2} \sigma \quad (3.21)$$

$$\rightarrow \sigma_{a\chi} = \frac{2}{3} \left( \frac{\pi R^2}{N_a} \right) = \frac{2}{3} \sigma_{\text{sat}},$$

Hence with this convention, where  $\tau = 1$  for  $\sigma_{a\chi} = \sigma_{\text{sat}} = \pi R^2/N_a$ .

This leads to the full integral for the probability of energy loss sufficient for capture after  $N$  scatters,

$$g_N(w) = \int_0^1 dz_1 \int_0^1 dz_2 \cdots \int_0^1 dz_N \Theta\left(v_{esc} \prod_{i=1}^N (1 - z_i \beta_+)^{-1/2} - w\right). \quad (3.27)$$

One common simplification of the above expression is to assume the kinematic factor  $z$  assumes its average value throughout (sometimes this is an ok assumption if  $\tau \gg 1$ , but see [25] for a discussion of form factors in white dwarfs),  $\langle z_i \rangle \approx 1/2$ , in which case  $g_N(z)$  simplifies to a theta function

$$g_N(w) = \Theta\left(v_{esc}(1 - \langle z_i \rangle \beta_+)^{-N/2} - w\right). \quad (3.28)$$

Using this estimate for  $g_N(w)$ , the  $N$  scatter capture equation becomes

$$C_N \simeq \pi R^2 p_N(\tau) \frac{\sqrt{6} n_X}{3\sqrt{\pi \bar{v}}} \left( (2\bar{v}^2 + 3v_{esc}^2) - (2\bar{v}^2 + 3v_N^2) \exp\left\{ \left( -\frac{3(v_N^2 - v_{esc}^2)}{2\bar{v}^2} \right) \right\} \right), \quad (3.29)$$

where  $v_N = v_{esc}(1 - \beta_+/2)^{-N/2}$ . If we further assume that  $v_{esc} \gg \bar{v}$  and  $m_X \gg m$ , we find

$$C_N = \sqrt{24\pi} p_N(\tau) G n_X M R \frac{1}{\bar{v}} \left( 1 - \left( 1 + \frac{2A_N^2 \bar{v}^2}{3v_{esc}^2} \right) e^{-A_N^2} \right); \quad A_N^2 = \frac{3v_{esc}^2 N m}{\bar{v}^2 m_X}. \quad (3.30)$$

### 3.4 Redshifted kinetic energy

While the above scattering capture is generally applicable, there is a subtlety to capture in the case that the spacetime around the capturing star is sufficiently curved. In this case, in the rest frame far from the star, the dark matter's kinetic energy will be diminished by a redshift factor  $\chi = 1/[1 - (1 - 2GM/R)^{1/2}]$ , meaning it is somewhat more difficult for the dark matter to drop below escape velocity while scattering. One way to account for this it so make the substitution in Eq. (3.28)

$$v_{esc} \rightarrow \sqrt{2\chi}, \quad (3.31)$$

where this will appropriately rescale the effective escape velocity from the vantage of a distant observer to account for the gravitational redshift effect.

## 4 Thermalization, Heating, and Other Effects in Astrophysical Bodies

We now turn to the configuration dark matter settles into, and the effects dark matter can have after becoming bound to a star (planet/asteroid/gas cloud/dragon/etc). This will necessarily be the least complete section of this introduction to dark matter in astrophysical bodies, and it is good to emphasize why. In this section, we begin to say what effect dark matter will have on astrophysical objects, but our understanding of this is only as good as our models of the astrophysical objects themselves. As previously mentioned, there is a rich history of looking at astrophysical objects and wondering if some hitherto un-modeled feature of these objects might be attributed to dark matter [20].

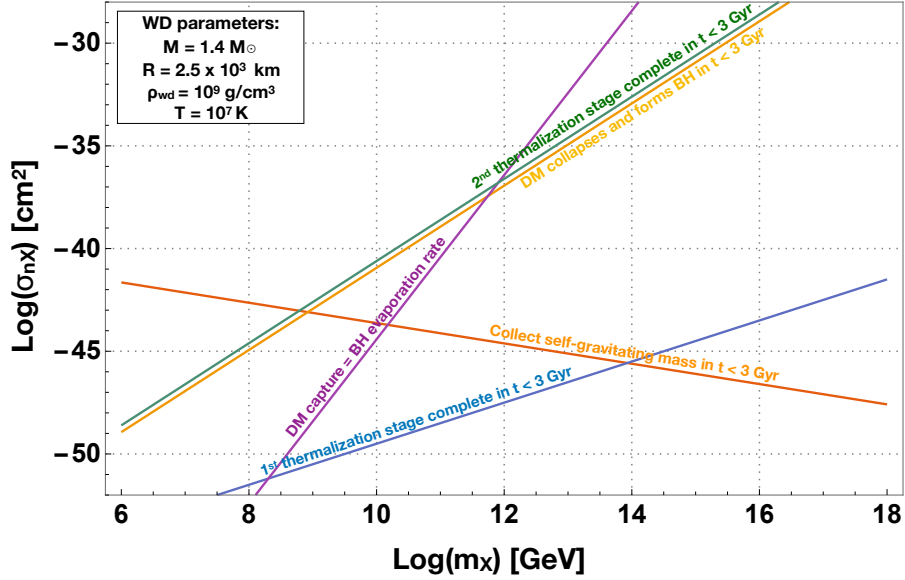


Figure 12: Thermalization timescales for heavy dark matter in a white dwarf from [10].

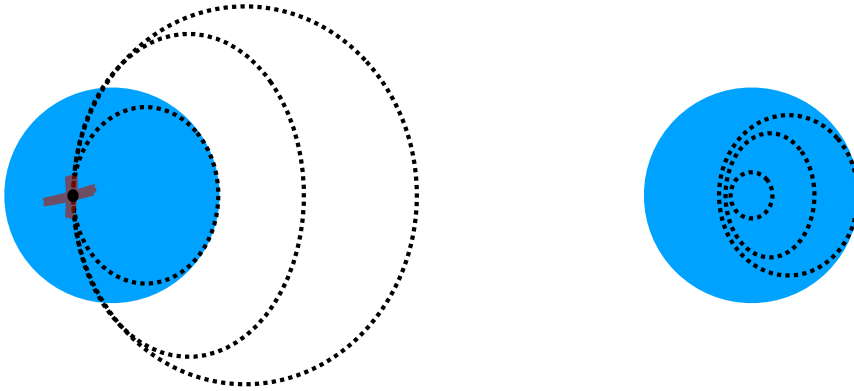


Figure 13: Illustration of thermalization times in an astrophysical object. The left shows first thermalization, when the dark matter scatters until its orbit through the star is fully contained. By the end of second thermalization shown on the right, dark matter will have the same temperature as the star’s interior, orbiting around the so-called “thermalization radius.”

## 4.1 First thermalization

After dark matter is captured on an orbit through the star, it will re-scatter with the star until it settles into an orbit fully contained within the star. For a detailed review of thermalization see [5]. The first thermalization time is typically much shorter than other relevant timescales. For

the sun,  $t_1$  thermalization from scattering off protons with cross-section  $\sigma_{p\chi}$  is

$$t_1 = \frac{\pi R_\odot^{3/2} m_\chi}{\tau_\odot m_j \sqrt{GM_\odot}} \int_{\frac{2m_p}{m_\chi}}^1 \frac{d\epsilon}{\epsilon^{3/2} (2.38 - \epsilon)}$$

$$\simeq 4.9 \times 10^7 \text{ yrs} \times \left( \frac{m_\chi}{10^7 \text{ GeV}} \right)^{3/2} \left( \frac{10^{-54} \text{ cm}^2}{\sigma_{p\chi}} \right), \quad (4.1)$$

Where the dimensionless variable giving the energy loss rate during  $t_1$  thermalization is  $\epsilon \equiv \frac{E}{m_\chi} \frac{R}{GM}$ .

## 4.2 Second thermalization

After the dark matter enters an orbital trajectory fully contained in the star, it will continue to scatter until its kinetic energy matches the thermal energy of the star,

$$\frac{dE}{dt} \simeq -\rho_a \sigma_{a\chi} v_\chi^3, \quad (4.2)$$

where the final energy in the integral is fixed by dark matter's ‘‘thermalized’’ energy  $E_{th} \approx \frac{3}{2} T_a$ .

There are two important exceptions to this treatment to note

1. If dark matter has an extremely high cross-section with the object, it may slow to a speed below the thermal speed of the object's particles  $a$ . This is the so-called viscous regime where  $v_a \gg v_\chi$ , and requires some special consideration to determine the drift time of dark matter to the object's core [5].
2. Likewise, if the object is made of a degenerate fluid (*e.g.* a neutron star), both the capture rate [26] and the thermalization times [27, 28] will need to be carefully re-considered.

After second thermalization, the dark matter will reside within the ‘‘thermalization radius,’’ which is a zone defined by applying the virial theorem,  $2 \langle E_{kin} \rangle = - \langle V \rangle$ , for the dark matter's kinetic and potential energy,  $\langle E_{kin} \rangle = \frac{3}{2} T_a$  and  $\langle V \rangle = -\frac{4}{3} \pi r_{th}^2 \rho_a G m_\chi$ . For the sun and the Earth this thermalization radius is [5]

$$r_{th} = \sqrt{\frac{9T_a}{4\pi G \rho_a m_\chi}} \approx 30 \text{ km} \times \left( \frac{10^7 \text{ GeV}}{m_\chi} \right)^{\frac{1}{2}} \left( \frac{T_\odot}{1.5 \times 10^7 \text{ K}} \right)^{\frac{1}{2}} \left( \frac{156 \text{ g/cm}^3}{\rho_\odot} \right)^{\frac{1}{2}}$$

$$\approx 2 \text{ km} \times \left( \frac{10^7 \text{ GeV}}{m_\chi} \right)^{\frac{1}{2}} \left( \frac{T_\oplus}{5 \times 10^3 \text{ K}} \right)^{\frac{1}{2}} \left( \frac{10 \text{ g/cm}^3}{\rho_\oplus} \right)^{\frac{1}{2}}. \quad (4.3)$$

## 4.3 Heating and other Effects

After dark matter is captured in astrophysical objects, it can have a number of observable effects.

- **Heating:** If dark matter annihilates or kinetically heats (from its halo kinetic energy or the energy gained during infall) [29] inside the star, this can result in a late-time temperature for the star according to

$$m_\chi C_\chi = 4\pi \sigma_B R^2 T_a^4, \quad (4.4)$$

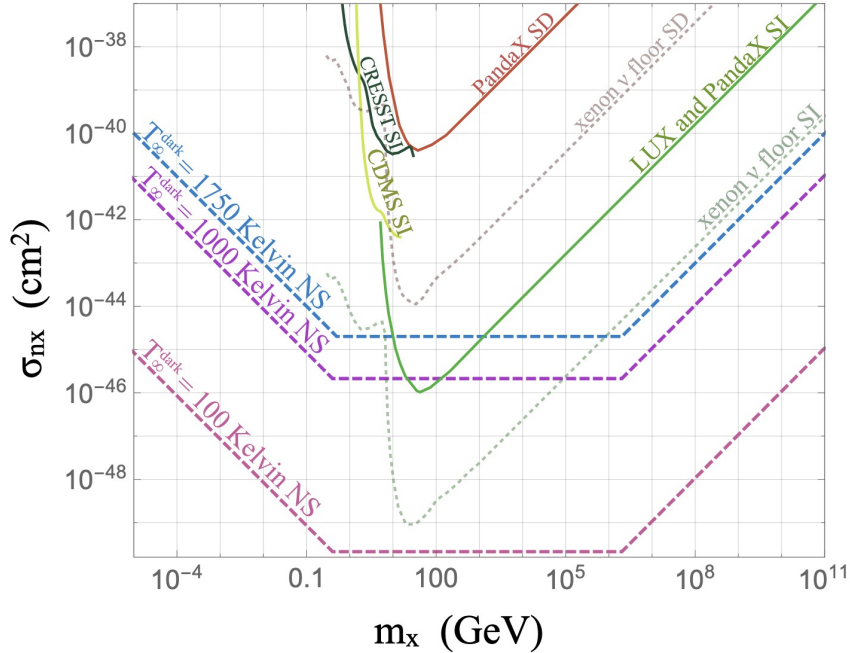


Figure 14: Potential sensitivity to dark matter heating for a neutron star within hundreds of parsecs of Earth [29].

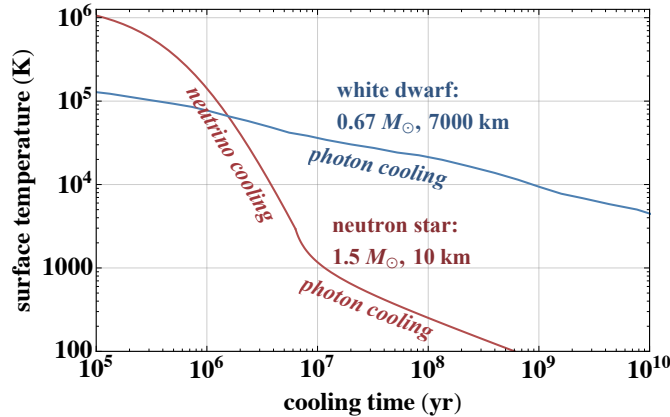


Figure 15: Cooling curves for a white dwarf and a neutron star from [30]. The white dwarf and neutron stars have mass and radius indicated, and the above assumes no heating from dark matter. This can be compared to the predicted late time temperatures that can be imparted from dark matter, discussed in the text.

where  $\sigma_B = \pi^2/60$  is the Stefan-Boltzmann constant in natural units, we assume the dark matter heating is the major contributor to the star's thermal energy, and this is the result for an isothermal spherical blackbody. This is actually pretty close to the correct result for an old neutron star, except the LHS of this equation becomes  $\gamma_{vesc} m_\chi C_\chi$ , and the RHS gains a factor of  $(1 - 2GM/R)$  from relativistic effects. Note also that, even if dark matter does not annihilate in a neutron star, it still heats it considerably by an amount up to  $(\gamma_{vesc} - 1)m_\chi C_\chi$  [29]. The sensitivity for this is shown in Figure 14.

Figure 15 shows the late time cooling behavior for a standard white dwarf and neutron star. In practice the white dwarf will have a richer interior thermal structure at late times – the asymptotic temperature from dark matter annihilation heating for the white dwarf parameters shown in Figure 15 is given by [30, 31],

$$T_{\text{WD}} \approx 4000 \text{ K} \left( \frac{350 \text{ km/s}}{v_{\text{rel}}} \right)^{1/4} \left( \frac{\rho_{\chi}}{10^3 \text{ GeV/cm}^3} \right)^{1/4}, \quad (4.5)$$

- **Black hole formation:** It has been appreciated for some time that if dark matter is a particle under some particle-anti-particle asymmetry (aka asymmetric just like visible matter), it can form black holes in astrophysical objects. The basic dynamic is that once enough dark matter collects into a radius  $r_{th}$  given by Eq. (4.3), the thermalized dark matter sphere can become unstable to collapse, then collapse and form a black hole [32]. During such a collapse it can also cause white dwarfs to ignite [8, 10].

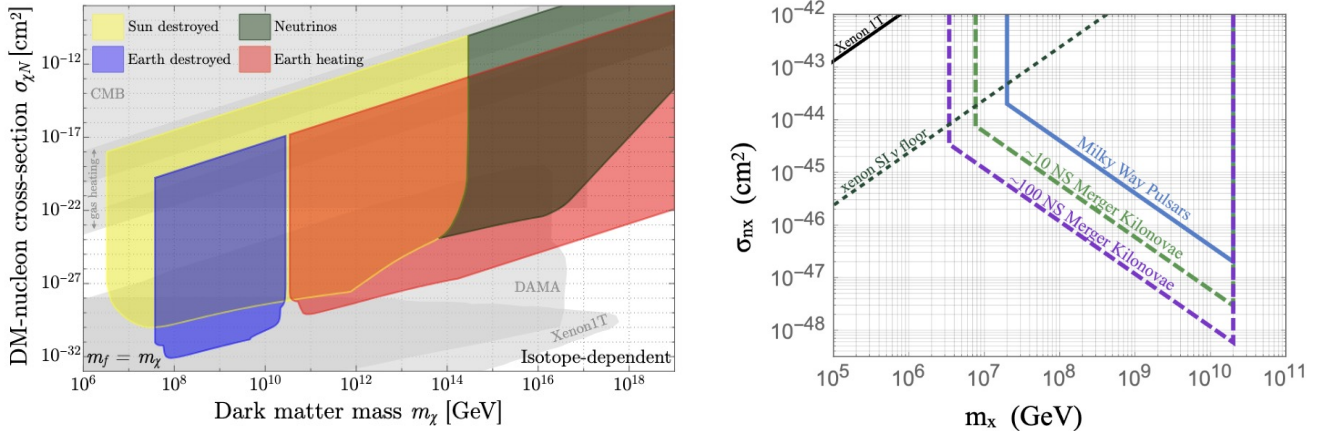


Figure 16: Regions of sensitivity for the Earth and Sun from [5] (left) and neutron stars from [33] (right) resulting from dark matter forming black holes in their interiors.

The black holes that can result from the dark matter collapsing in the astrophysical objects' interiors will either grow to consume these objects, or evaporate and deposit energy. The black hole growth is determined by [5]

$$\frac{dM_{\text{BH}}}{dt} = \frac{4\pi\rho_*(GM_{\text{BH}})^2}{c_{s*}^3} + e_{\chi}m_{\chi}C_{\chi} - \frac{f(M_{\text{BH}})}{(GM_{\text{BH}})^2}, \quad (4.6)$$

where the first term should be the familiar Bondi accretion rate, for the object's sound speed  $c_{s*}$ , the second term accounts for further dark matter accretion onto the black hole with efficiency  $e_{\chi}$ , relative to its collection in the astrophysical body, and the final term accounts for Hawking evaporation of the black hole, with  $O(1)$  greybody factors  $f(M_{\text{BH}})$ . Of course, the possibility that dark matter may be converting compact stars to black holes is exciting – there are some interesting astrophysical anomalies that might be associated with this phenomenon [33–35]. Figure 16 shows some parameter space where astrophysical objects have sensitivity to black hole formation in their interiors.

# A Kinematics

## A.1 Elastic scattering review

Let the two particles have masses  $m_1$  and  $m_2$ , and relative speed  $v$ , with particle 2 at rest in the lab frame. The CM-velocity will then be

$$V_{\text{cm}} = \frac{m_1 v}{m_1 + m_2}.$$

In CM frame (primed), the initial speeds are

$$v'_{1i} = v - V_{\text{cm}} = \frac{m_2}{m_1 + m_2} v, \quad v'_{2i} = -\frac{m_1}{m_1 + m_2} v.$$

Elasticity in the CM frame implies  $v'_{2f} = v'_{2i} = \frac{m_1}{m_1 + m_2} v$ . Let  $\theta_{\text{cm}}$  be the angle between  $v'_{1i}$  and  $v'_{1f}$ . Particle 2's final lab-frame velocity is the vector sum of the CM velocity shift (let's put it in the x-direction) plus its CM-frame recoil velocity:

$$\mathbf{v}_{2,\text{lab}} = V_{\text{cm}} \hat{\mathbf{x}} - v'_{2f} [\cos(\theta_{\text{cm}}) \hat{\mathbf{x}} + \sin(\theta_{\text{cm}}) \hat{\mathbf{y}}].$$

Hence

$$v_{2,\text{lab}}^2 = V_{\text{cm}}^2 + v_{2f}'^2 - 2 V_{\text{cm}} v_{2f}' \cos \theta_{\text{cm}} = 2 \left( \frac{m_1}{m_1 + m_2} v \right)^2 [1 - \cos \theta_{\text{cm}}].$$

using  $v_{2f}' = \frac{m_1}{m_1 + m_2} v$  and  $V_{\text{cm}} = \frac{m_1}{m_1 + m_2} v$ .

The recoil energy of  $m_2$  in the lab frame is

$$E = \frac{1}{2} m_2 v_{2,\text{lab}}^2 = \frac{1}{2} m_2 2 \left( \frac{m_1}{m_1 + m_2} v \right)^2 [1 - \cos \theta_{\text{cm}}] = E_i \frac{2 m_1 m_2}{(m_1 + m_2)^2} [1 - \cos \theta_{\text{cm}}],$$

where  $E_i = \frac{1}{2} m_1 v^2$  is the initial kinetic energy of  $m_1$ . Using  $1 - \cos \theta_{\text{cm}} = 2 \sin^2(\frac{\theta_{\text{cm}}}{2})$ , we get

$$E = E_i \frac{4 m_1 m_2}{(m_1 + m_2)^2} \sin^2\left(\frac{\theta_{\text{cm}}}{2}\right).$$

## A.2 Distribution of recoil energy

We have found that the recoil energy of particle  $m_2$  in the lab frame is related to the CM scattering angle  $\theta_{\text{cm}}$  by

$$E = E_{\text{max}} \sin^2\left(\frac{\theta_{\text{cm}}}{2}\right), \quad \text{with} \quad E_{\text{min}} = 0, \quad E_{\text{max}} = E_i \frac{4 m_1 m_2}{(m_1 + m_2)^2}.$$

In the CM frame, scattering is isotropic so the probability to scatter into the solid angle  $d\Omega_{\text{cm}}$  is equally distributed

$$dP = \frac{d\Omega_{\text{cm}}}{4\pi} = \frac{1}{2} \sin \theta_{\text{cm}} d\theta_{\text{cm}},$$

where we have integrated out the  $\phi$  component of the solid angle since scattering occurs in a plane,  $d\Omega_{\text{cm}} = 2\pi \sin \theta_{\text{cm}} d\theta_{\text{cm}}$ .

Now we differentiate  $E$  and use  $\sin \theta \cos \theta = \frac{1}{2} \sin(2\theta)$ ,

$$dE = E_{\text{max}} \sin\left(\frac{\theta_{\text{cm}}}{2}\right) \cos\left(\frac{\theta_{\text{cm}}}{2}\right) d\theta_{\text{cm}} = \frac{E_{\text{max}}}{2} \sin \theta_{\text{cm}} d\theta_{\text{cm}},$$

and from this we find that the probability distribution for energy transfer from  $1 \rightarrow 2$  is equally distributed from 0 to  $E_{\text{max}}$ ,

$$dP = \frac{dE}{E_{\text{max}}}, \quad P(E) = \frac{dP}{dE} = \frac{1}{E_{\text{max}}} \quad \text{for} \quad 0 \leq E \leq E_{\text{max}}.$$

## References

- [1] XENON collaboration, E. Aprile et al., *Low-Energy Nuclear Recoil Calibration of XENONnT with a  $^{88}\text{YBe}$  Photoneutron Source*, [2412.10451](#).
- [2] J. I. Collar, *Applications of an  $^{88}\text{Y}/\text{Be}$  photo-neutron calibration source to Dark Matter and Neutrino Experiments*, *Phys. Rev. Lett.* **110** (2013) 211101, [[1303.2686](#)].
- [3] G. D. Mack, J. F. Beacom and G. Bertone, *Towards Closing the Window on Strongly Interacting Dark Matter: Far-Reaching Constraints from Earth's Heat Flow*, *Phys. Rev.* **D76** (2007) 043523, [[0705.4298](#)].
- [4] J. Bramante, A. Buchanan, A. Goodman and E. Lodhi, *Terrestrial and Martian Heat Flow Limits on Dark Matter*, *Phys. Rev.* **D101** (2020) 043001, [[1909.11683](#)].
- [5] J. F. Acevedo, J. Bramante, A. Goodman, J. Kopp and T. Opferkuch, *Dark Matter, Destroyer of Worlds: Neutrino, Thermal, and Existential Signatures from Black Holes in the Sun and Earth*, *JCAP* **04** (2021) 026, [[2012.09176](#)].
- [6] H. N. Pollack, S. J. Hurter and J. R. Johnson, *Heat flow from the earth's interior: Analysis of the global data set*, *Reviews of Geophysics* **31** (1993) 267–280.
- [7] J. H. Davies and D. R. Davies, *Earth's surface heat flux*, *Solid Earth* **1** (2010) 5–24.
- [8] J. Bramante, *Dark matter ignition of type Ia supernovae*, *Phys. Rev. Lett.* **115** (2015) 141301, [[1505.07464](#)].
- [9] P. W. Graham, S. Rajendran and J. Varela, *Dark Matter Triggers of Supernovae*, *Phys. Rev.* **D92** (2015) 063007, [[1505.04444](#)].
- [10] J. F. Acevedo and J. Bramante, *Supernovae Sparked By Dark Matter in White Dwarfs*, *Phys. Rev.* **D100** (2019) 043020, [[1904.11993](#)].
- [11] N. Raj, *Supernovae and superbursts by dark matter clumps*, [2306.14981](#).
- [12] D. Maoz and F. Mannucci, *Type-Ia supernova rates and the progenitor problem, a review*, *Publ. Astron. Soc. Austral.* **29** (2012) 447, [[1111.4492](#)].
- [13] D. Maoz, F. Mannucci and G. Nelemans, *Observational clues to the progenitors of Type-Ia supernovae*, *Ann. Rev. Astron. Astrophys.* **52** (2014) 107–170, [[1312.0628](#)].
- [14] R. A. Scalzo, A. J. Ruiter and S. A. Sim, *The ejected mass distribution of type Ia supernovae: A significant rate of non-Chandrasekhar-mass progenitors*, *Mon. Not. Roy. Astron. Soc.* **445** (2014) 2535–2544, [[1408.6601](#)].
- [15] Y. C. Pan et al., *The Host Galaxies of Type Ia Supernovae Discovered by the Palomar Transient Factory*, *Mon. Not. Roy. Astron. Soc.* **438** (2014) 1391–1416, [[1311.6344](#)].
- [16] D. N. Spergel and W. H. Press, *Effect of hypothetical, weakly interacting, massive particles on energy transport in the solar interior*, *Astrophys. J.* **294** (1985) 663–673.

- [17] W. H. Press and D. N. Spergel, *Capture by the sun of a galactic population of weakly interacting massive particles*, *Astrophys. J.* **296** (1985) 679–684.
- [18] L. M. Krauss, K. Freese, W. Press and D. Spergel, *Cold dark matter candidates and the solar neutrino problem*, *Astrophys. J.* **299** (1985) 1001.
- [19] A. Gould, *WIMP Distribution in and Evaporation From the Sun*, *Astrophys. J.* **321** (1987) 560.
- [20] A. B. McDonald, *Solar neutrinos*, *New J. Phys.* **6** (2004) 121, [[astro-ph/0406253](#)].
- [21] M. LoVerde and M. Zaldarriaga, *Neutrino clustering around spherical dark matter halos*, *Phys. Rev. D* **89** (2014) 063502, [[1310.6459](#)].
- [22] N. Bozorgnia, A. Fattahi, C. S. Frenk, A. Cheek, D. G. Cerdeno, F. A. Gómez et al., *The dark matter component of the Gaia radially anisotropic substructure*, *JCAP* **07** (2020) 036, [[1910.07536](#)].
- [23] L. Necib and T. Lin, *Substructure at High Speed. II. The Local Escape Velocity and Milky Way Mass with Gaia eDR3*, *Astrophys. J.* **926** (2022) 189, [[2102.02211](#)].
- [24] E. Shima, T. Matsuda, H. Takeda and K. Sawada, *Hydrodynamic calculations of axisymmetric accretion flow*, *Mon. Not. Roy. Astron. Soc.* **217** (Nov., 1985) 367–386.
- [25] J. Bramante, A. Delgado and A. Martin, *Multiscatter stellar capture of dark matter*, *Phys. Rev. D* **96** (2017) 063002, [[1703.04043](#)].
- [26] J. F. Acevedo, J. Bramante, R. K. Leane and N. Raj, *Cooking Pasta with Dark Matter: Kinetic and Annihilation Heating of Neutron Star Crusts*, [1911.06334](#).
- [27] R. Garani, A. Gupta and N. Raj, *Observing the thermalization of dark matter in neutron stars*, *Phys. Rev. D* **103** (2021) 043019, [[2009.10728](#)].
- [28] B. Bertoni, A. E. Nelson and S. Reddy, *Dark Matter Thermalization in Neutron Stars*, *Phys. Rev. D* **88** (2013) 123505, [[1309.1721](#)].
- [29] M. Baryakhtar, J. Bramante, S. W. Li, T. Linden and N. Raj, *Dark Kinetic Heating of Neutron Stars and An Infrared Window On WIMPs, SIMPs, and Pure Higgsinos*, *Phys. Rev. Lett.* **119** (2017) 131801, [[1704.01577](#)].
- [30] J. Bramante and N. Raj, *Dark matter in compact stars*, *Phys. Rept.* **1052** (2024) 1–48, [[2307.14435](#)].
- [31] R. Garani, N. Raj and J. Reynoso-Cordova, *Could compact stars in globular clusters constrain dark matter?*, [2303.18009](#).
- [32] I. Goldman and S. Nussinov, *Weakly Interacting Massive Particles and Neutron Stars*, *Phys. Rev. D* **40** (1989) 3221–3230.
- [33] J. Bramante, T. Linden and Y.-D. Tsai, *Searching for dark matter with neutron star mergers and quiet kilonovae*, *Phys. Rev. D* **97** (2018) 055016, [[1706.00001](#)].

- [34] J. Bramante and T. Linden, *Detecting Dark Matter with Imploding Pulsars in the Galactic Center*, *Phys. Rev. Lett.* **113** (2014) 191301, [1405.1031].
- [35] J. Bramante and N. Raj, *Cosmology of self-replicating universes in the interior of black holes formed by dark matter-seeded stellar collapse*, *Phys. Rev. D* **110** (2024) 043537, [2405.12277].